Macromolecular Materials and Engineering
www.mame-journal.de

Influence of Block Copolymer Concentration and Resin Crosslink Density on the Properties of UV-Curable Methacrylate Resin Systems

*Martin Demleitner, Florian Schönl, Jörg Angermann, Pascal Fässler, Iris Lamparth, Kai Rist, Thomas Schnur, Yohann Catel, Sabine Rosenfeldt, Markus Retsch, Holger Ruckdäschel, and Volker Altstädt**

Additive manufacturing is on the verge of replacing established processes in dentistry, as it offers the possibility of manufacturing individual parts simply and cost-effectively. Due to its suitability for a wide variety of materials and, above all, its high precision, the focus is currently on stereolithographic processes. Intrinsic brittleness of the used multifunctional acrylic monomers remains however one of the major challenges. One promising concept is the use of block copolymers (BCPs) guaranteeing minor effects on 3D-printing processing and UV-curing due to initially at least partial solubility, and hence low viscosity impact. A polycaprolactone-polysiloxane (PCL-PDMS-PCL) triblock copolymer is synthesized via ring-opening polymerization of caprolactone and used in radical UV-cured methacrylic resin systems. Small angle X-ray scattering measurements reveal the self-assembly of the BCPs to objects of around 20 nm prior to curing. Subsequently, thermo-mechanical characterization is carried out by dynamic mechanical analysis, flexural testing, and fracture toughness measurements (K_{IC}). Transmission electron microscopy and scanning electron microscopy micrographs show a homogenous distribution of the BCPs and effective toughening via cavitation and shear yielding. The influence of the crosslink density on the toughness and the high effectiveness of block copolymers for improving fracture toughness is clearly shown.

1. Introduction

In recent years, additive manufacturing has become established in numerous industries both for prototype manufacturing and small scale production. It is increasingly important in dentistry, as it enables a fast and cost-effective way to produce individual parts. With its high precision and processing speed, stereolithography has established itself in dentistry.[1,2] 3D-printing materials such as tooth models, orthodontic workpieces (e.g., splints), wax models for metal casting and press ceramics, denture bases, and denture teeth are already available in the market.[3–5] Today, dentures are manufactured in a multistep process starting with the preparation of a wax model which is then used to create a plaster mold using the lost wax technique. The denture is then prepared by thermal polymerization of a freshly made mixture of poly(methyl methacrylate) (PMMA) powder with a methyl methacrylate (MMA)-based liquid in that mold under pressure in a water bath. Direct additive manufacturing of

M. Demleitner, F. Schönl, H. Ruckdäschel, V. Altstädt
Department of Polymer Engineering
University of Bayreuth
Universitätsstr. 30, 95447 Bayreuth, Germany
E-mail: volker.altstaedt@uni-bayreuth.de

J. Angermann, P. Fässler, I. Lamparth, K. Rist, T. Schnur, Y. Catel
Ivoclar Vivadent AG
Bendererstrasse 2, Schaan 9494, Principality of Liechtenstein

S. Rosenfeldt, M. Retsch
Department of Physical Chemistry I and Bavarian Polymer Institute (BPI)
University of Bayreuth
Universitätsstr. 30, 95447 Bayreuth, Germany

The ORCID identification number(s) for the author(s) of this article can be found under https://doi.org/10.1002/mame.202200320

DOI: 10.1002/mame.202200320

dentures could eliminate the many tedious manual steps in a fully digital process. The development of 3D-printing denture bases is particularly challenging as these materials must exhibit high mechanical properties (high flexural strength and modulus) as well as high fracture toughness.[6] Due to the low reactivity and high volatility of MMA, conventional MMA-based denture base materials are hardly suitable for 3D printing and stereolithographic resins therefore mainly consist of dimethacrylates.

However, dimethacrylate-based materials often exhibit a significantly higher crosslink density than thermally cured step-growth resin systems, and thus exhibit brittle material behavior prone to catastrophic failure.[6,7] Due to the high crosslinking, no pronounced plastic deformation can occur prior to failure as no rearrangement or orientations of the chains can take place, as it is typically the case with thermoplastic materials (crazing, necking). As a result, toughening technologies are required to enable 3D printing of tough dimethacrylate-based denture materials. To date, various strategies for the toughening of dimethacrylate networks have been investigated.

It is well-known that radical-cured, chain-growth systems show greater network heterogeneity due to free chain ends and a broader molecular weight distribution. In addition, higher internal stresses develop during curing due to early gelation.[8] By using new monomers and monomer combinations or adding thiol-enes, the network can be directly tailored toward higher fracture toughness or impact strength.[9,10] Beigi et al. showed that with the addition of thiol-enes, the fracture toughness of bisphenol A-glycidyl methacrylate/triethylene glycol dimethacrylate (Bis-GMA/TEGDMA) increased with 30% thiol-ene from 0.8 to 1.8 $MPam^{0.5}$ by forming a more homogenous network.[11] This can be explained by the fact that the thiol-enes trigger a regulated step-growth polymerization that shifts the gel point to a higher conversion, allowing more stress relaxation. However, a disadvantage is the costly development work, as well as the unpleasant odor and limited storage stability of these formulations.[12]

In radical-cured systems, thermoplastic particles, e.g., polyethylene particles can be used to increase fracture toughness, but in some cases significant amounts have to be added.[13] The same applies for rubber particles[14–16] or fibers.[17,18] This limits processing due to the high viscosity but also leads to lower monomer conversion and thus poorer mechanical properties. Significantly better characteristic values at lower concentrations are shown by so-called core–shell rubber particles (CSRs). Increases in fracture toughness or impact strength of up to 100% for photocurable resin systems with relatively low concentrations are possible.[19–23]

The fracture mechanisms at work here are debonding/cavitation of the particles, followed by plastic void growth which allows the formation of shear bands. If CSR matrix adhesion is sufficient, internal stresses are generated which elastically stretch the particle until failure occurs. Difficulties with CSR arise in achieving homogenous dispersion as they tend to agglomerate and deteriorating efficiency in highly cross-linked resin systems. Other side effects of CSR can include an increase in viscosity which makes processing more difficult and increased opacity of materials due to light scattering of the agglomerates.

Another class of toughness modifiers represent block copolymers (BCPs) which consist of at least two covalently bonded, chemically distinct, polymer blocks. Typically, one of the blocks is miscible, and therefore compatible with the resin, while the other block is immiscible. Due to the covalent bonding, the blocks cannot separate macroscopically, and phase separation is limited to the size of the individual blocks, resulting in what is known as microphase separation.

BCPs in resin systems as toughener were first described in 1997 and have been used very successfully for epoxy resin systems.[24] The poly(ethylene oxide)-*b*-(butylene oxide) (PEO-PBO) diblock copolymer, commonly known as *Fortegra 100* from Olin Corporation,[25] is particularly efficient. Other examples include Arkema's *Nanostrength* series based on poly(methyl methacrylate)-poly(butyl acrylate) (PMMA/PBuA) blocks[26,27] or BCPs based on polycaprolactone-polydimethylsiloxane (PCL-PDMS).[28] In epoxy resins, an increase of the work of fracture of up to 20 times in comparison to unmodified resin was mentioned. Another advantage is the good compatibility with the resin system during the mixing process, and thus easier process control.[29] Here, either self-assembly takes place before curing or the blocks arrange themselves in nanoscale domains during the curing according to the polarity change of the system, the so-called polymerization-induced phase separation (PIPS).[30] The mechanisms of self-assembly are based on the equilibrium thermodynamics of the initial resin system. However, PIPS is kinetically controlled with competing reactions between polymerization and phase separation, making precise control of the desired morphology challenging. The morphology of self-assembling BCP systems can be more easily controlled by parameters such as BCP concentration, block length and ratio, interaction parameters between blocks or with the matrix system, and others.[31]

The very small change in polarity in free-radical curing systems often leads to a significant reduction in the efficiency of PIPS-based block copolymers, since parts remain dissolved in the system and act as internal plasticizers and, instead of increasing toughness, tend to decrease modulus, strength, and glass transition temperature T_g. For example, Paz et al. used commercially available PMMA-PBuA block copolymers (*Nanostrength M52* from Arkema) in PMMA.[27] However, no significant toughness enhancing effect was observed, most likely due to unsuccessful microphase separation in the acrylate resin system. Also for peroxide-cured, unsaturated polyesters, modifications with commercially available poly(ethylene oxide)/poly(propylene oxide) PEO-PPO-PEO block copolymers (*Pluronics* from BASF) were accompanied by only a rather small increase in fracture toughness but a sharp drop in modulus.[32] Redline et al. investigated different poly(ethylene propylene)-poly(ethylene oxide) (PEP-PEO) block copolymers in dicumyl peroxide-cured Bis-GMA/PEGDMA mixtures and demonstrated an increase in fracture toughness of up to 100% due to wormlike structures.[33] These nanostructures show one of the most pronounced increases of the fracture toughness in acrylic resin systems.[25,29] However, the standard deviation of the obtained fracture toughness was quite high indicating heterogenous network and a high percentage of remaining double bonds (maximum degree of cure around 80%) which complicates the evaluation of the BCP influence. They linked the rather poor toughenability to network defects and different network formation mechanisms. Small-angle X-ray scattering (SAXS) measurements showed that self-assembly of the block copolymers on nanometer scale

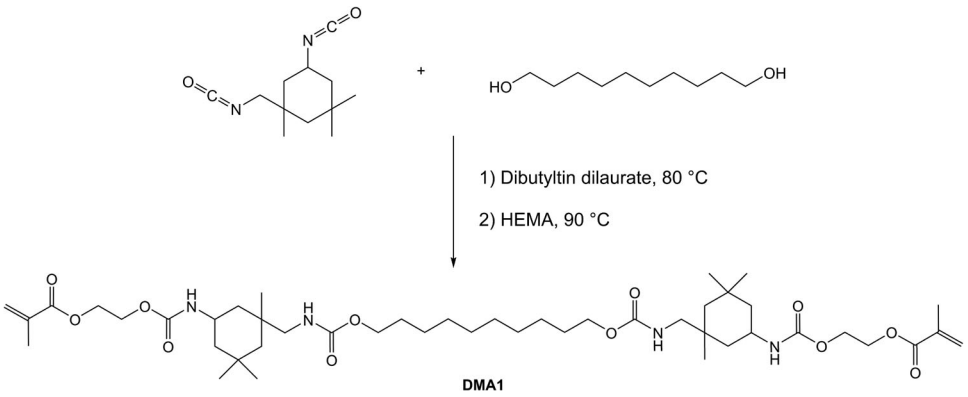

Figure 1. Synthesis pathway of monomer DMA1.

already occurred before curing. Therefore, it is assumed, that for photocurable resin systems, BCPs with self-assembly behavior prior to UV-cure are preferred to avoid only partial phase separation. Here, rapid network formation will efficiently constrain the self-assembled nanostructures, "freezing" the current structure, and preventing reorganization during curing.

Analogous to CSR particles in resin systems, cavitation occurs of the block copolymers during interaction with the crack tip, allowing the formation of shear bands that have an energy-dissipating effect. Due to the up to an order of magnitude smaller domains (up to 15 nm) compared to CSR (often around 200 nm), significantly higher increases in fracture toughness are possible by so-called "nanocavitation".[34]

So far, BCPs as toughening agents for UV-curable resin systems have rarely been investigated in the literature. As far as the authors are aware, there is only one publication focusing on thin coating applications (100 µm) with a cationic curable epoxy resin.[35] Here, however the poly(ethylene oxide)/poly(glycidyl methacrylate) PEO-PGMA diblock copolymers used actually showed a significant decrease in fracture toughness of up to 27% compared to the neat resin system. This was explained by relatively low molar mass of the BCPs which limits the possibility of phase separation. SAXS measurements confirmed the lack of phase separation. The impact of the crosslink density on the fracture behavior and toughenability of the resin system was mainly investigated for epoxy resin systems.[36–38] Here, it was clearly shown that, in general, the lower the crosslink density, the stronger the toughening effect.

The aim of this work is to use block copolymers synthesized by anionic ring-opening polymerization to increase the fracture toughness of UV-cured dimethacrylate networks with low crosslinking density. In this context, a mixture of the urethane dimethacrylate (DMA1) and 2-phenoxyethyl methacrylate (PEMA) was selected as monomer mixture (various DMA1/PEMA ratios were considered). Urethane groups were incorporated into the structure of the dimethacrylate to improve both the mechanical properties and the polymerization rate. A PCL-PDMS-PCL block copolymer was chosen as toughener, since PDMS is typically incompatible in methacrylate mixtures. Moreover, excellent results with such toughenes were obtained in epoxy resins.[28,39] The influence of the amounts of BCP on both the fracture toughness and the mechanical properties of UV-cured materials based on different DMA1/PEMA ratios is discussed. The impact of the crosslinking density on these parameters has also been investigated.

2. Results and Discussion

2.1. Synthesis of DMA1

DMA1 was synthesized by successive addition of 1,10-decanediol and 2-hydroxyethyl methacrylate (HEMA) to 2-isophorone diisocyanate (IPDI, **Figure 1**). Due to the difference in reactivity of the primary and secondary isocyanate groups of IPDI, 1,10-decanediol reacts mainly with the primary isocyanate group in the first step, while HEMA adds to the remaining secondary isocyanate group in the second step. Monitoring of the reaction by IR spectroscopy showed that all isocyanate groups were consumed during the reaction. No vibration band was detected in the area around 2200 cm^{-1}. A broad absorption at 3335 cm^{-1} together with a strong one at 1526 cm^{-1} was assigned to NH groups, a very strong absorption at 1695 cm^{-1} to carbonyl groups and a middle-weak absorption at 1638 cm^{-1} to double bonds. DMA1 was isolated in excellent yield (99%) as a colorless resin.

2.2. Synthesis of PCL-PDMS-PCL Block Copolymer

The bisaminopropyl-terminated polydimethylsiloxane block was synthesized by base-catalyzed ring-opening polymerization of octamethylcyclotetrasiloxane with 1,3-bis(3-aminopropyl) tetramethyldisiloxane and tetramethylammonium-3-aminopropyl dimethylsilanoate as catalyst at 80 °C (**Figure 2**). The molecular weight of 3200 g mol^{-1} was adjusted by employing octamethylcyclotetrasiloxane and the aminopropyl disiloxane in a molar ratio of 11:1 and was confirmed by proton NMR spectroscopy. Removal of volatile by-products under vacuum yielded 88% of the PDMS(3200) block as a clear liquid. The subsequent anionic ring-opening polymerization of *ε*-caprolactone at 130 °C was catalyzed by tin(II) 2-ethylhexanoate. The PCL(1600)-*b*-PDMS(3200)-*b*-PCL(1600) block copolymer was obtained in 96% yield as an off-white, waxy solid. The molecular weight and block were chosen according to the promising results reported in the literature for PCL-PDMS-PCL triblock copolymers.[28,40]

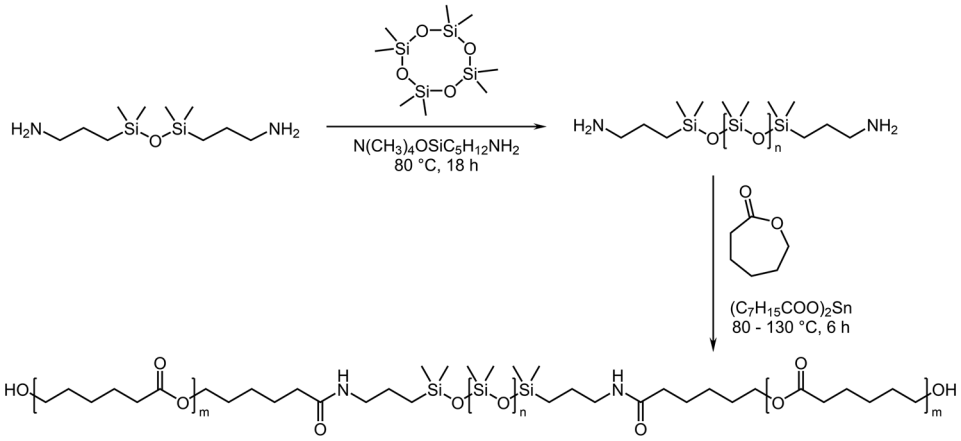

Figure 2. Synthesis of the PCL-*b*-PDMS-*b*-PCL block copolymer.

2.3. BCP Morphology before and after UV-Curing

According to the literature, it is highly preferable for radically cured resin systems to exhibit preaggregation or self-assembly of BCPs prior to curing to ensure efficient toughening.[33,35] Prior to UV-curing, all blends are homogenous and transparent indicating that no macroscopic phase separation has occurred to an extent that exceeds the wavelength of visible light. Since visual inspection is insensitive to possible nanophase separation, nanostructural analysis was performed using SAXS. Based on the knowledge that PDMS is immiscible in dimethacrylate and PCL is miscible, the BCP is expected to form a nanophase separation, associated with different excess electron densities of the two polymer blocks. While common SAXS studies used BCP contents ≥10 wt% and addressed morphological changes of BCP during superlattice formation,[41] we focus on the influence of the addition of low concentrations of BCP (≤10 wt%). At low concentrations, only single BCP particles with core–shell structure or small individual aggregates should occur, but no super-structuring of BCPs.[41] In other words, in our study the phase structure is expected to have no clear periodical distance due to well-defined BCP–BCP self-assemblies, and therefore no higher-order Bragg reflexes of such an arrangement.[66]

The SAXS data of the uncured resin system containing different concentration of BCP, exemplarily shown for the 50:50 blend, are presented in **Figure 3**. More information about the evaluation of the SAXS data is given in the Supporting Information.

All resin samples exhibit a power law of approximately q^{-3} in region I ($q < 0.01$ Å^{-1}). This scaling is already present in the neat resin, and hence, mainly a structural characteristic of the resin morphology. After addition of BCP, the scattering patterns of the formulations evolve a shoulder in region II ($q > 0.01$ Å^{-1}). The shoulder intensity scales with the amount of added BCP. Applying Guinier's law led to a radius of gyration of $R_g \sim 7.5$ nm, which corresponds to a radius R of ≈10 nm in case of spherical particles.[42,43] We also measured the characteristic interaction distance for the phase-separated bulk BCP case and found a reasonable agreement ($d \approx 20$ nm $\approx 2R$) (Figure S1, Supporting Information). Thus, the shoulder indicates the existence of identical nanoscaled regions in the different systems, proving the presence of a BCP nanophase separation prior to curing, which is considered essential for efficient toughening. Most likely, this specific BCP nanophase separation is caused by the PDMS block (insoluble in resin). Note, that the radius of ≈10 nm is consistent with the transmission electron microscopy (TEM) result (**Figure 4**) of cured resin formulations, which revealed well-defined mainly spherical objects of the same size. In a more detailed look, one notices that the cross-over point between regions I and II (Figure 3) shifts slightly with increasing BCP content from ≈0.010 Å^{-1} (3 wt%) to ≈0.015 Å^{-1} (10 wt%). This hints to an increase of the correlation length L_c from about 60 to ≈80 nm.

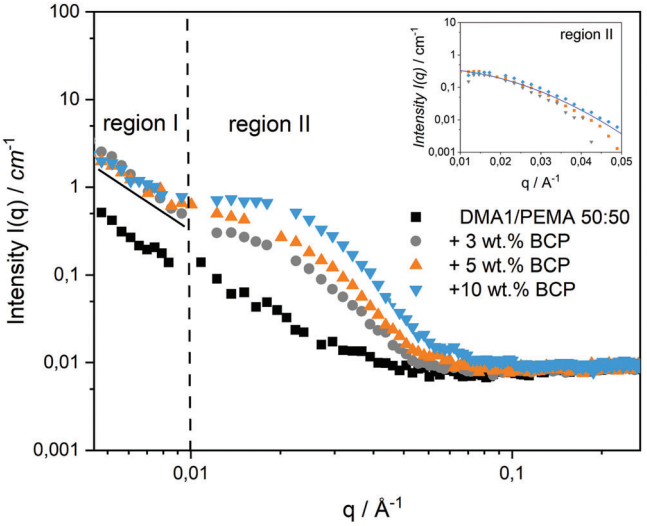

Figure 3. SAXS data (symbols) of 50:50 blend with different amount of BCP (black: 0 wt% (neat), blue: 10 wt%, orange: 5 wt%, and gray: 3 wt%) in the uncured state. Experimental data are shown without background subtraction. Additionally, a black line demonstrating a q^{-3} power law is given. The inset shows the data in region II after subtraction of the neat scattering contribution (as background) and normalization to 5 wt% BCP. The data are well described by a Guinier approximation (blue line).

Even if we miss well-defined Bragg reflections indicative for the formation of highly ordered superstructures, the change in L_c may be an indication for the onset of higher-ordered structures due to BCP–BCP long-range interaction. Changes in L_c may originate from different averaged BCP cluster sizes. We hypothesize

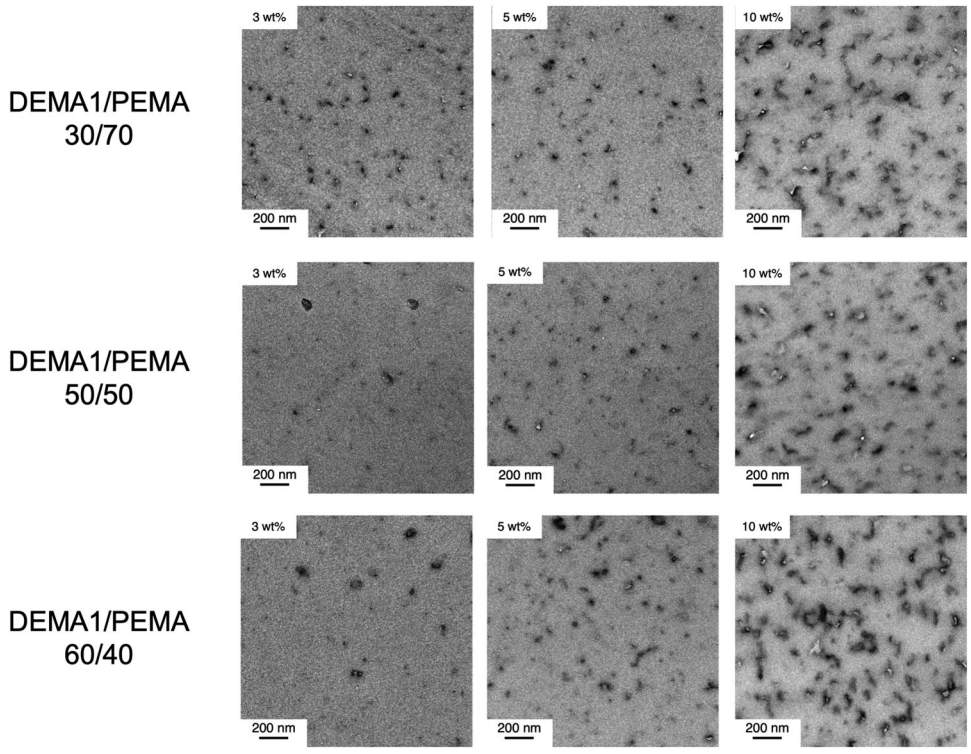

Figure 4. TEM micrographs of cured formulation containing different amount of BCPs.

that during stirring the BCP wax in the resin gel, nanophase separated individual units of the BCP with $R_g \sim 7.5$ nm aggregate to clusters, which grow in size with increasing BCP content.

SAXS measurements on the cured system show similar features in region II (Figure S2, Supporting Information) demonstrating that clusters are formed before and are being retained during the UV-curing process.

Representative TEM micrographs of the cured resin formulations are shown in Figure 4. They reveal that up to a concentration of 5 wt%, the BCPs self-assemble into well-dispersed (spherical) objects with an average diameter of ≈20 nm. As the concentration increased, the number of small BCP particles increased while at 10 wt% bigger cluster/coagulated nanoparticles with a size up to 100 nm are seen, similar to the observation made by Wang et al.[41] These results in terms of domain size and clusters are in good agreement with the SAXS measurements.

2.4. Degree of Cure and Network Properties

The degree of cure (DoC) is a crucial factor for the final properties of the material, especially for chain-growth polymerization such as UV-curing resin systems where the network is not fully formed until the late stages of curing. The DoC depends on factors such as oxygen inhibition,[44] photoinitiator and pigment concentration,[45] or monomer functionality[46] and can lead to formulations with uncured monomers and cure gradients within the sample. The degree of cure was determined by Raman spectroscopy[47,48] which, in contrast to IR spectroscopy, is more sensitive to homo-nuclear bonds such as the C=C double bond in the vinyl ester group.

Here, the double bond signal (1638 cm^{-1}) for each formulation in the uncured and cured state was normalized to the vibrational aromatic ring signal from the 2-phenoxyethyl methacrylate at 1460 cm^{-1}. The degree of cure of each blend system was therefore comparable regardless of BCP concentration.

Figure 5 shows the degree of cure determined across each compact tension (CT) specimen width. High conversions (>95%) are visible for all formulations, assuming low amounts of residual monomers. It is clear that the higher the amount of PEMA, the higher the DoC or double bond conversion. This result was expected and is due to the higher monomer reactivity and the lower crosslinking density of the network.

It is visible that for the 60/40 and 50/50 blends, oxygen inhibition occurs within the first 100–300 µm resulting in a small, but not significant, cure gradient (see insets). The content of block copolymer seems to have only slight impact on the degree of cure at higher concentrations, proving once more the nanophase separation behavior and thus the low blocking and scattering of UV light.

Dynamic mechanical analysis (DMA) measurements were performed to determine the thermo-mechanical profile of the resin blend formulations and the influence of BCP content on storage and Young's modulus, T_g, and crosslink density. As shown in the literature, BCPs can be an effective approach for toughening resin systems without deteriorating the thermo-mechanical properties. DMA measurements can also provide insight into the phase separation behavior and morphology based on the shift in T_g, broadening of tan(δ) peaks (ratio of loss to

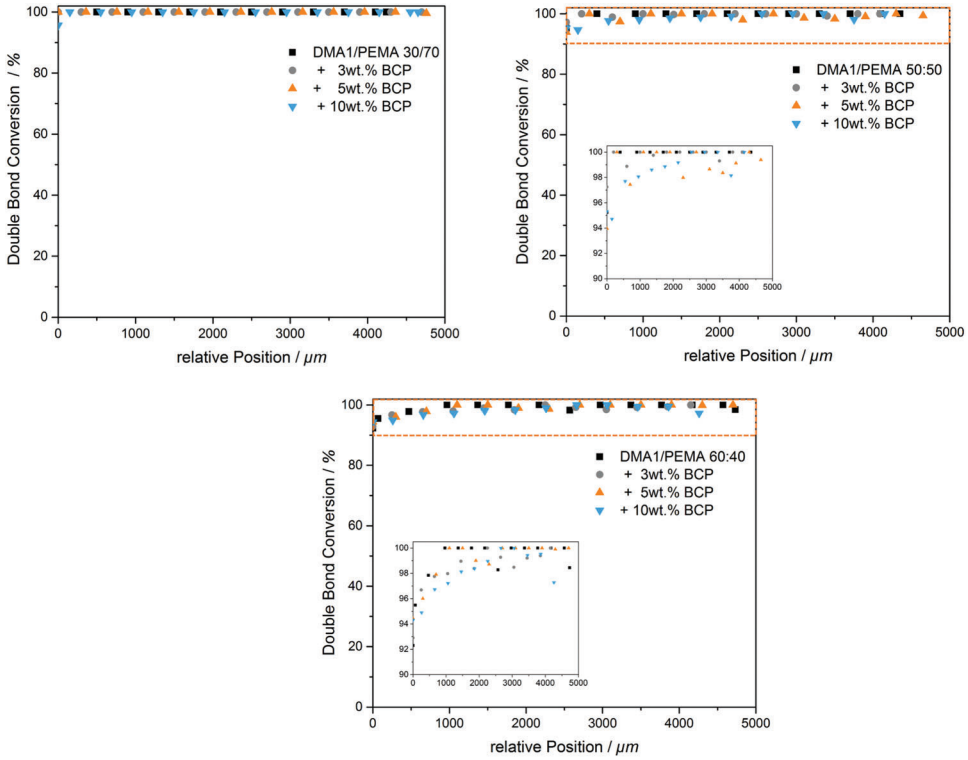

Figure 5. Degree of conversion (%) as a function of the specimen width and BCP concentration for the different resin formulations. The inset shows the data points in the region 90% to 100% double bond conversion (dashed orange box).

storage, e.g., damping), and height variation.[49] Here, the miscible block of BCP may act as plasticizer leading to reduction of T_g and storage modulus. In the case of PDMS-PCL block copolymers, both flexible blocks can act as plasticizers, depending on the content and length of the block copolymer as already shown in the literature.[50,51] **Figure 6** shows the evolution of storage modulus and loss factor as a function of temperature at different amounts of BCP for each blend formulation. First, it can be seen that as the content of monofunctional monomer PEMA decreases, the T_g increases from 73 °C for the 30:70 blend to 86 °C for the 50:50 blend and to 95 °C for the 60:40 blend. This can be related to a higher crosslink density with higher content of DMA1. A slight drop in T_g can be seen for all BCP toughened blend systems, which is more pronounced with increasing BCP content.

Compared to the neat resin system, the addition of BCP shows a drop in modulus at room temperature (RT) and rubbery modulus (T_g+30 K), especially for the formulations containing 10 wt% BCP. This results in lower crosslink density values (determined with Equation (1)) with a reduction up to 29% for the 50:50 blend, 45% for the 60/40 blend, and 38% for the 30/70 blend. Coagulation or rather clusters at higher BCP content (shown in TEM, Figure 4) may be responsible for this behavior.

Furthermore, slightly reduced degree of cure, as demonstrated by Raman, could contribute to this effect since in the radical-cured chain-growth polymerization, the complete network is formed only in the very last stages of the curing reaction. It is noteworthy that the tan(δ) values remain fairly constant, albeit well above 1, indicating high damping due to comparatively low network densities. This proves the high mobility of the polymer chains.

In conclusion, the reduction of glass transition temperature and tan(δ) shift was not very pronounced, which shows that the block copolymers have only a small effect on the thermomechanical properties of the resin systems, especially up to 5 wt%. The values obtained from the DMA measurements are summarized in **Table 1**.

2.5. Mechanical Properties and Toughening Effect

The interaction of a large number of components and different UV-curing conditions, as well as the fact that most UV-curing systems are still only used for coatings and thin films, often makes mechanical characterization and evaluation very complex. For a deeper insight, we refer to other publications[52–55] and focus on the influence of the BCP toughener on the mechanical properties. Since toughening of brittle polymers is often accompanied by an undesirable loss of stiffness and strength, three-point bending tests were carried out to determine the effect of varying BCP content on flexural modulus and strength. The results are shown in **Figure 7**. For a given BCP content, higher DMA1 content leads to higher flexural strength and modulus. This trend can be explained by the different crosslinking densities as well as the presence of more urethane groups. For all resin systems, the flexural strength and flexural modulus decrease with the addition of BCP. Surprisingly, this effect was more pronounced for the low-crosslinked 30:70 system, leading to 70% of the initial modulus

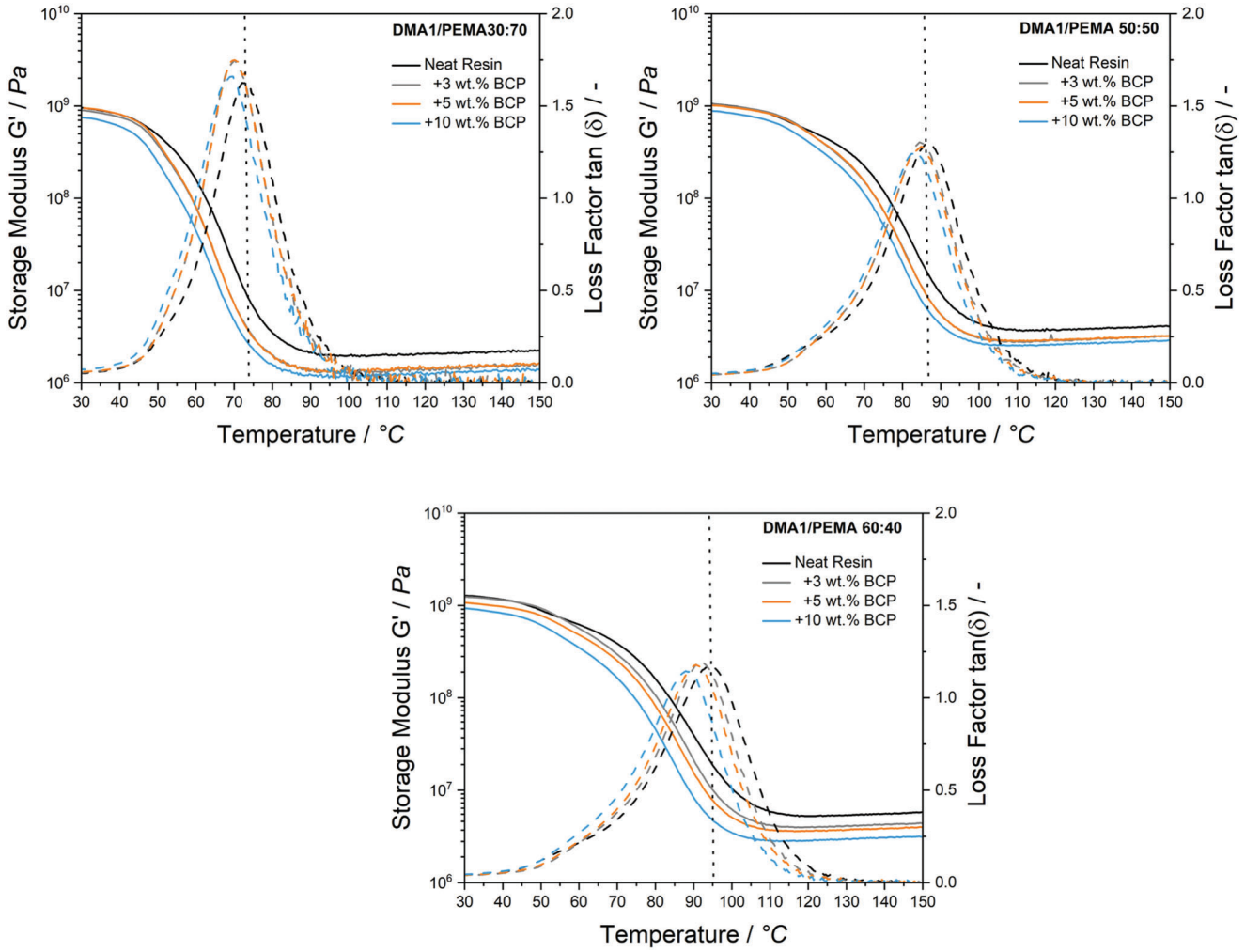

Figure 6. DMA graphs of BCP-modified resin systems (solid: storage modulus, dashed: loss factor, black dotted line: guidance for T_g of neat resin systems).

Table 1. Overview of resin parameter obtained by DMA measurements.

Resin system	T_g [°C]	Young's modulus [GPa]	Rubber modulus at $T_g + 30$ K [Pa]	Crosslink density ν [mol m^{-3}]
DMA1/PEMA: 30/70	73	2.60	1.96E6	627.4
+3 wt% BCP	70	2.45	1.35E6	435.6
+5 wt% BCP	70	2.58	1.36E6	438.0
+10 wt% BCP	69	2.03	1.20E6	387.8
DMA1/PEMA: 50/50	87	2.87	3.64E6	1121
+3 wt% BCP	85	2.85	2.83E6	877
+5 wt% BCP	85	2.77	2.88E6	892
+10 wt% BCP	84	2.41	2.56E6	794
DMA1/PEMA: 60/40	94	3.47	5.27E6	1594
+3 wt% BCP	92	3.36	3.97E6	1209
+5 wt% BCP	90	2.91	3.62E6	1104
+10 wt% BCP	88	2.54	2.84E6	873

and 50% of the initial strength at 10 wt% BCP, while 76% and 60% were retained for the 60:40 blend system, respectively. For the 50:50 system, the addition of 10 wt% BCP resulted in 72% of the original modulus and 55% of the original strength. However, at a BCP content of up to 5 wt% BCP content, the decrease in both strength and modulus is much less pronounced reaching a maximum decrease of 25%. The loss of modulus is expected due to the low moduli of the incorporated PCL-PDMS blocks. Similar trends have already been observed after the addition of BCPs in epoxy resin systems.[56–58]

The critical stress intensity factor K_{IC} and work of fracture G_{IC} of the dimethacrylate resin systems as function of BCP content are represented in **Figure 8**. The cured materials that do not contain any BCP exhibited very low K_{IC} and G_{IC} values. The DMA1/PEMA ratio did not affect the fracture toughness, as the three mixtures (70/30, 50/50, and 40/60) had similar K_{IC} and G_{IC} values. Similar results have been reported in the literature for neat epoxy resins.[38]

However, it is evident that the addition of BCP improves the fracture toughness for all crosslink densities. Interestingly, even

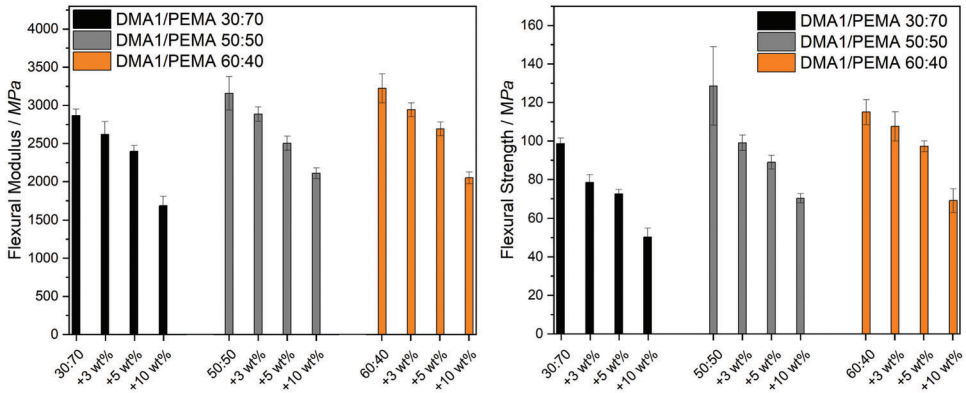

Figure 7. Flexural modulus (left) and flexural strength (right) of the BCP-toughened resin systems.

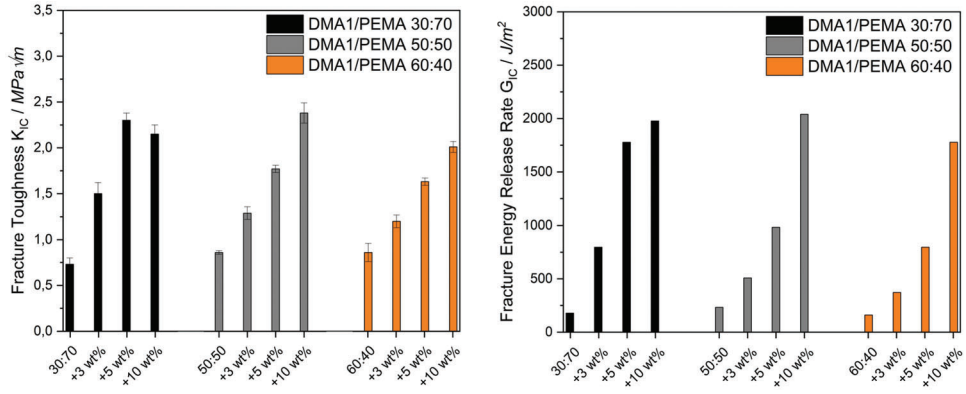

Figure 8. Fracture toughness and fracture energy release rate of BCP-toughened resin systems.

the addition of a relatively small amount of 3 wt% leads to a remarkable improvement in fracture toughness by up to 100%. For 5 wt% in particular, the 30:70 system with low crosslink density (CLD) showed three times higher values than the neat system. As expected, the intrinsically lower crosslink density showed better performance than the other two systems. With lower crosslink density, it is assumed that higher energy dissipation is possible in combination with BCPs. It is generally known that higher G_{IC} and K_{IC} values at lower concentration are possible for crosslinkable systems with higher ductility, based, e.g., on lower crosslink density or more flexible crosslinks, in contrast to more rigid or higher-crosslinked systems.

At 10 wt%, a relatively modest increase in fracture toughness is seen compared to 5 wt% which actually leads to a decrease in the case of the 30:70 system. This can be linked to agglomeration/coagulation, lowering the effective particle concentration. It therefore appears that a BCP content of 5 wt% is the best concentration to maintain the initial flexural modulus and strength, more than doubling the fracture toughness while increasing the work of fracture by a factor of four.

Scanning electron microscope (SEM) micrographs of the fracture surfaces of the broken CT specimen of neat and BCP-toughened formulations are shown in **Figure 9**. The neat formulations show plain and smooth surfaces typical for brittle failure. However, the low CLD system, the neat 30:70 blend, showed slightly rougher surfaces compared to the other neat formulations, indicating more intrinsic ductile behavior.

Compared to the neat formulations, all BCP-modified systems showed a very coarse and rough surface indicating significant crack resistance and energy dissipation effects. In all formulations, the spherical morphology of BCP with a size of about 20 nm is visible. The main toughening mechanism is likely to be the particle-matrix debonding through cavitation and subsequent shear yielding. These mechanisms have already been investigated in detail for BCP-toughened epoxy resins.[34,59] For formulations with 10 wt% BCP, agglomerates and/or coagulates apparently reduce the effective transfer of stress between the matrix and the particles, thereby leading to lower fracture toughness enhancement. The 30:70 blend with lower crosslink density showed a significantly rougher surface than the other formulations, regardless of BCP concentration.

It is interesting to note that the presence of BCP leads to higher fracture toughness, but at the expense of crosslink density and modulus. For the 30:70 with low crosslink density, the decrease is significantly lower in comparison to the highly crosslinked 60:40 blend system. Since the rigid matrix is partially replaced by quite flexible PCL and PDMS blocks, this is expected as shown in the literature for PEP-PEO block copolymers.[60] However, as mentioned above, the impact on flexural properties is more pronounced for the low-crosslinked resin system. In general, a level

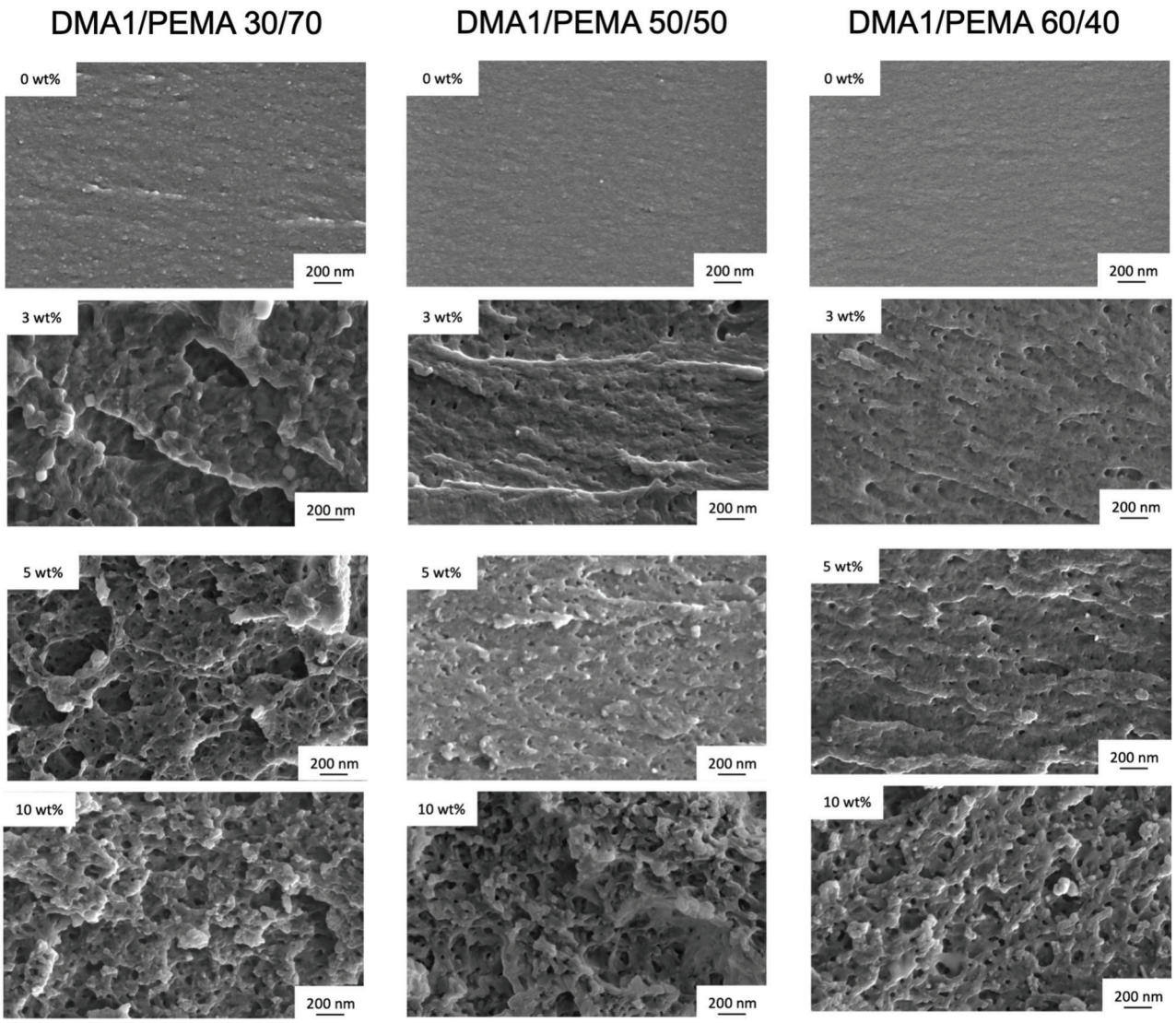

Figure 9. SEM micrographs of fracture surfaces of neat and BCP-toughened resin systems.

of 5 wt% of BCP, especially for the 50:50 systems, seems to be the most promising to achieve a balance between toughness and strength as well as modulus. **Figure 10** shows the different systems and their characteristic values summarizing these results.

3. Summary and Outlook

In this work, a PCL-PDMS-PCL block copolymer was efficiently synthesized in two steps and used as a toughness modifier in UV-cured methacrylate resin systems with low crosslink density. Using SAXS, it was shown that the addition of the BCP to the methacrylate mixture led to the formation of self-assembled, spherical clusters. The BCP content did not significantly affect the nanomorphology observed in TEM. The synthesized BCP proved to be an excellent toughness modifier for the selected methacrylate resins. The addition of BCP resulted in a significant increase in fracture toughness and work of fracture. Higher BCP contents not only lead to increased fracture toughness, but also to a decrease in the mechanical properties (flexural strength and modulus) of the resin. Therefore, 5 wt% BCP seems to be an optimal amount. It has also been shown that the crosslink density of the dimethacrylate resin has a great influence on the toughening efficiency. It is known that the higher the base toughness of the resin to be modified, the higher the efficiency of a toughness modifier.[61] For a given amount of BCP, the lower the crosslink density of the base resin, the higher the increase in toughness. In general, it can be said that the conclusion of Redline et al.,[33] and their assumption of challenging BCP toughening of radical-cured resin systems due to heterogenous network structure, is not entirely accurate. In this work, it has been shown that radical-cured resin systems can indeed be efficiently toughened with BCP depending on the nature and content of BCP and resin crosslink density.

For the future, other nanophase-separated morphologies could even be more promising in increasing fracture toughness.

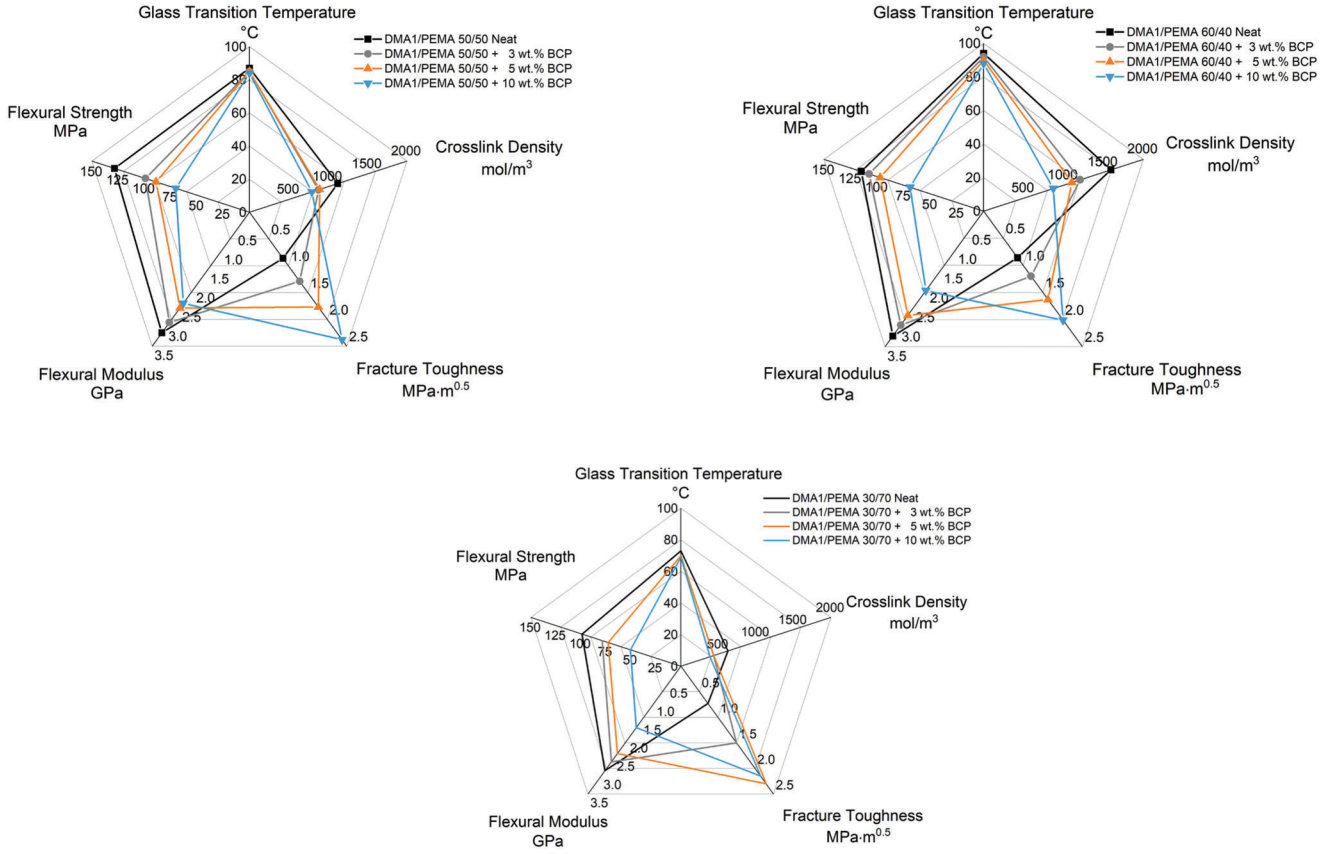

Figure 10. Spider web diagrams with selected properties of the investigated BCP-toughened dimethacrylate resin systems.

As demonstrated for step-growth epoxy resins, wormlike morphologies are particularly interesting and should be pursued in UV-curable resin systems.[25,29,50,62,63] Such morphologies might be obtained via the variation of the block copolymer structure (length/nature of the blocks, block ratio, etc.). More work is needed to fully understand the physical nature of self-assembly and the interaction of BCPs with the resin network. Last but not least, the processability and final properties of the resin systems presented here should be investigated in 3D-printing experiments.

4. Experimental Section

Materials: 1,10-decanediol (Impag AG, Switzerland), IPDI (TCI Europe, Germany), HEMA (Evonik Performance Materials GmbH, Germany), and dibutyltin dilaurate (Brenntag Schweizerhall AG, Switzerland) were used as received. 1,3-Bis(3-aminopropyl)tetramethyldisiloxane, octamethylcyclotetrasiloxane, *ε*-caprolactone, and tin(II) 2-ethylhexanoate were purchased from abcr (Germany). 2-phenoxyethyl methacrylate (PEMA) was purchased form Sartomer (France) and was used as received. Diphenyl(2,4,6-trimethylbenzoyl)phosphine oxide (TPO) was purchased from Rahn (Germany). All other reagents were purchased from Sigma-Aldrich (Switzerland) and were used as received. All reactions concerning Si-polymers were performed under an argon atmosphere.

Synthesis of the Urethane Dimethacrylate DMA 1: A mixture of 1,10-decanediol (489.2 g, 2.81 mol), IPDI (1247.9 g, 5.61 mol), and dibutyltin dilaurate (1.2 g) was heated to 40 °C. The diol dissolved completely, and the temperature was increased to ≈100 °C. After the exotherm subsided, the mixture was stirred for 1 h at 80 °C and a mixture of HEMA (730.6 g, 5.61 mol) and butylated hydroxytoluene (BHT, 0.74 g) was slowly added. After stirring at 90 °C for 10 min, the total consumption of isocyanate was proven by IR spectroscopy. DMA1 (2460 g) was obtained as a colorless resin. Yield: 99%.

^{1}H NMR (400 MHz, $CDCl_3$): δ (ppm) = 0.85–0.97, 1.01–1.06, 1.19–1.38, and 1.59–1.75 [4 m, 46H, $(CH_2)_8$, $CH_{2,\,cycl.}$, $CH_{3,\,cycl.}$), 2.03 (s, 6H, $CH_{3,\,methacryl}$), 2.81–2.98 and 3.20–3.33 (2 m, 4H, NCH_2), 3.65–3.88 [m, 2H, NCH], 3.98–4.11 (m, 4H, $OCH_2(CH_2)_8$), 4.26–4.40 (m, 8H, $O(CH_2)_2O$), 4.57–4.94 (m, 4H, NH), 5.60 and 6.14 (2 s, 2H each, $=CH_2$).

^{13}C NMR (100 MHz, $CDCl_3$): δ (ppm) = 18.3 ($CH_{3,\,methacryl}$), 23.2, 27.6, and 35.0 ($CH_{3,\,cycl.}$), 25.9, 29.0, 29.2, and 29.4 [$(CH_2)_8$], 31.8 and 36.4 ($C_{cycl.}$), 41.8, 46.4, and 47.0 ($CH_{2,\,cycl.}$), 44.5 and 44.7 (NCH), 54.9 (NCH_2), 62.4, 62.6, 62.9, 64.8, and 65.0 (OCH_2), 126.0 ($C{=}CH_2$), 136.0 ($C{=}CH_2$), 155.3, 156.0, 156.6, and 157.2 ($C{=}O_{urethane}$), 167.2 ($C{=}O_{methacryl}$).

IR (diamond ATR): ν (cm^{-1}) = 3341 (br, NH), 2927 and 2856 (m, C–H), 1695 (vs C=O), 1638 (m, C=C), 1526 (s, NH), 1456 (m, CH_2, CH_3), 1366 (m, CH_3), 1236 (C–N), 1167 and 1039 (s, m, COC), 942 (m, =CH), 774 [m, $(CH_2)_8$].

Synthesis of the PCL-b-PDMS-b-PCL Block Copolymer. *Synthesis of tetramethylammonium-3-aminopropyl dimethylsilanoate*: A mixture of 1,3-bis(3-aminopropyl)tetramethyldisiloxane (2.49 g, 10.0 mmol) and tetramethylammonium hydroxide pentahydrate (3.62 g, 20 mmol) in tetrahydrofuran (THF; 10 mL) was heated at reflux for 3 h. The solvent was evaporated, and the residue was heated to 50 °C under vacuum. The yellowish residue was recrystallized from THF (20 mL). 3.17 g (15.4 mmol; 77%) of a white solid was obtained.

^{1}H NMR ($CDCl_3$, 400 MHz): δ = 3.16 (s, 12H; N^+–CH_3), 2.37 (t, J = 7.1 Hz, 2H; N–CH_2), 1.28 (m, 2H; CH_2), 0.14 (m, 2H; Si–CH_2), –0.33 (s, 6H; Si–CH_3).

Synthesis of polydimethylsiloxane-α, ω-dipropyl-3-amine: PDMS(3200): A mixture of 1,3-bis(3-aminopropyl)tetramethyldisiloxane (4.98 g,

20.0 mmol) and octamethylcyclotetrasiloxane (12.00 g, 40 mmol) was heated to 80 °C. Tetramethylammonium-3-aminopropyl dimethylsilanoate (20 mg) was added and the reaction mixture was stirred at 80 °C. After 30 min, argon-saturated octamethylcyclotetrasiloxane (56.00 g, 0.192 mol) was slowly added. The reaction mixture was stirred at 80 °C for 18 h and then heated to 150 °C for 30 min in order to decompose the catalyst. Volatile components were removed under vacuum. 65.30 g (88 %) of a colorless oil was obtained.

^{1}H NMR (CDCl3, 400 MHz): $\delta = 2.64$ (t, $J = 7.0$ Hz; 4 Hz; N–CH_2), 1.43 (m, 4H; CH_2), 0.51 (m, 4H; Si–CH_2), 0.05 (s, 250H; Si–CH_3).

Synthesis of the PCL(1600)-b-PDMS(3200)-b-PCL(1600) block copolymer: A mixture of PDMS(3200) (20.00 g) and ϵ-caprolactone (20.40 g) was heated to 80 °C. After 1 h, tin(II) 2-ethylhexanoate (10 mg) was added and the bath temperature was gradually increased to 130 °C in increments of 10 °C within 30 min. The reaction mixture was stirred at 130 °C for 5 h. Volatile components were evaporated under vacuum. 39.50 g (98%) of the block copolymer was obtained as a waxy, off-white solid.

^{1}H NMR ($CDCl_3$, 400 MHz): $\delta = 3.99$ (t, $J = 6.8$ Hz; 55H; O–CH_2), 3.57 (t, $J = 6.8$ Hz; 4H HO–CH_2), 3.15 (q, $J = 6.8$ Hz; 4H, N–CH_2), 2.24 (t, $J = 7.5$ Hz; 55H; C(O)–CH_2), 2.10 (t, $J = 7.5$ Hz; 4H; N–CH_2), 1.58 (m, 118H; CH_2), 1.32 (m, 59H; CH_2), 0.46 (m, 4H; Si–CH_2), 0.02 (s, 250H; Si–CH_3).

Materials and Sample Preparation: PEMA and the dimethacrylate DMA1 were used in weight ratios of 50/50, 40/60, and 70/30 to vary the crosslinking density. 1 wt% TPO was used as photoinitiator. The BCP was dispersed in the resin systems under magnetic stirring at 50 °C. The formulations were cured in stainless steel molds for the corresponding test specimens in a PrograPrint Cure UV-oven (Ivoclar Vivadent AG, Schaan, Liechtenstein) at a wavelength of 405 nm (intensity: 120 mW cm^{-2}) and 460 nm (intensity: 60 mW cm^{-2}) for 120 s (Program "Model"). After curing the first side, specimens were turned upside down and the lower side was cured with the same parameters. To reduce oxygen inhibition, the specimens were covered with a 50 µm poly(ethylene terephthalate) (PET) foil before cure.

Measurements and Characterization: *Nuclear Magnetic Resonance (NMR) spectroscopy*: NMR spectra were recorded on a DPX-400 (Bruker BioSpin) in deuterated chloroform ($CDCl_3$) with tetramethylsilane (TMS) as standard. Data are given in the following order: chemical shift in ppm; multiplicity (s, singlet; d, doublet; t, triplet; q, quartet; m, multiplet); coupling constant in Hertz (Hz); assignment. The molecular weight of the copolymer blocks was calculated from the proton NMR spectra by the determination of the number of repeating monomer units through calibration of the Si–CH_2 integrals of the aminopropyl groups. The NMR spectra can be found in the Supporting Information.

Fourier transform infrared spectroscopy (FTIR): An FTIR spectrometer Spectrum Two (Perkin Elmer) was used to record IR spectra of the monomer DMA1 and the PCL-*b*-PDMS-PCL block copolymer. The IR spectra can be found in the Supporting Information.

Scanning Electron Microscopy (SEM): To evaluate the mode of fracture, the fractured surfaces of the CT specimens were observed by Zeiss Leo 1530 SEM (Carl Zeiss AG, Oberkochen Germany) at an accelerating voltage of 3 kV. The specimens were gold coated by a sputter coater before SEM observations.

Tranmission Electron Microscopy (TEM): Samples were sectioned from the CT specimen with a diamond knife (Ultramikrotom Leica Model UC7) at ambient temperature. RuO_4 staining of the samples was carried out for 15 min. TEM measurements were performed with a Zeiss LEO EM922 Omega TM field emission energy filtering transmission electron microscope (FE-EFTEM) operated at an acceleration voltage of 200 kV. Zero-loss filtered micrographs ($\Delta E \sim 0$ eV) were recorded with a bottom mounted CMOS camera system (OneView, Gatan) and processed with DM 3.3 image processing software (Gatan).

Small angle X-rayScattering (SAXS): Measurements of SAXS data ("Double Ganesha AIR," SAXSLAB, Denmark) were performed at ambient conditions. In this laboratory-based system, X-rays were provided by a rotating copper anode (MicoMax 007HF, Rigaku Corporation, Japan; wavelength $\lambda = 1.54$ Å). A position-sensitive detector (PILATUS 300 K, Dectris) was used in different positions to cover a wide range of scattering vectors q ($q = 0.004$–0.6 Å^{-1}, $q = |\vec{q}| = \frac{4\pi}{\lambda}\sin(\frac{\theta}{2})$, with θ representing the scattering angle). Prior to the measurement, the resin formulations were filled in 1 mm glass capillaries (Hilgenberg, code 4007610). The radial intensity $I(q)$ was normalized to incident beam, a sample thickness of ≈1 mm, and acquisition time. Background correction was performed by subtracting the signal of a neat resin formulation.

Raman spectroscopy: An imaging system (WITec alpha 300 RA+) equipped with a spectrometer (UHTS 300 spectrometer, grating 600 groves mm^{-1}) and a back-illuminated camera (Andor Newton 970 EMCCD) with an electron multiplying charge-coupled device was used to determine the degree of cure. Measurements were performed using an excitation wavelength of $\lambda = 532$ nm together with a 10x objective (NA = 0.25), a laser intensity of 15 mW, an integration time of 0.5 s, and 50 accumulations. Each blend system was measured in uncured and cured state, and subsequently calibrated relative to the peak corresponding to the C=C bond to peak of the aromatic ring (1460 cm^{-1}) which stays constant during the polymerization. Each sample was screened across the complete width of the fracture surface of the CT specimen in 100 µm increments to determine potential cure gradients. Raman measurements were carried out within 24 h after fracture toughness measurements to avoid any influence of aging. All spectra were subjected to a cosmic ray removal routine and baseline correction using WITec project 5.3.

Dynamic Mechanical Analysis (DMA): DMA measurements were carried out at a heating rate of 3 K min^{-1} in torsional mode at an elastic deformation of 0.1% and an applied frequency of 1 Hz (Rheometrics Scientific ARES RDA III, Germany). The specimens had a rectangular shape with 50 × 10 × 2 mm[3] according to standard ISO 6721-7. The glass transition temperature was evaluated at the maximum of loss factor tan (δ) curve. The determined storage modulus in the rubbery plateau region could be considered inversely proportional to the chain length between crosslinks.[22,64] In order to calculate the crosslink density ν_c, Equation (1) was used

$$\nu_c = \frac{G'}{RT} = \frac{E'}{3RT} \tag{1}$$

where G' is the storage modulus obtained 30 °C beyond T_g, R is the gas constant (= 8.314 J mol^{-1} K^{-1}), E' is the Young's modulus, and T is the temperature 30 °C above T_g. Here, crosslink density is the moles of elastically effective network chains in unit volume.

Fracture toughness measurements: The fracture toughness of the material systems was evaluated by the critical stress intensity factor in mode I (K_{Ic} value) according to ISO 13586 with a universal testing machine (Zwick Z050, Zwick Roell, Ulm, Germany) using CT specimen. The initial crack was performed by tapping a razor blade into the notch. The initial load was set to 1 N and the testing speed to 10 mm min^{-1} with at least five specimens tested. After fracture, the exact crack length was measured from the fracture surfaces and the fracture toughness at crack initiation, and the critical stress intensity factor, K_{IC} was calculated by using the following equation

$$K_{IC} = \frac{F_m}{t\sqrt{w}} \cdot f\left(\frac{a}{w}\right) \tag{2}$$

where F_m is the maximum load at failure, t is the sample thickness, w is the overall length, a is the crack length, and $f(a/w)$ is a geometry factor according to ISO 13586.

Work of fracture G_{IC} was determined by using Equation (3)

$$G_{IC} = \frac{K_{IC}^2}{E} \cdot \left(1 - \nu^2\right) \tag{3}$$

where E is the modulus of elasticity determined from DMA measurements and ν is the Poisson ratio which was set to 0.37 for the methacrylate resin systems.[65] All measurements were carried out within 24 h after specimen preparation to avoid any influence of aging.

Flexural tests: Flexural properties were measured after storage of the cured samples (2 × 2 × 25 mm^3) at RT for 24 h. Three-point bending tests were carried out (span: 20 mm) with a speed of 0.8 mm min^{-1} using a

universal testing machine (Z2.5/TS, ZwickRoell, Germany), according to ISO 4049.

Supporting Information

Supporting Information is available from the Wiley Online Library or from the author.

Acknowledgements

Annika Pfaffenberger from the Department of Polymer Engineering for the TEM and SEM measurements is gratefully thanked. Furthermore, the authors express their gratitude to Dr. Holger Schmalz from the Department Macromolecular Chemistry II of the University of Bayreuth for performing the Raman experiments. After initial online publication, the chemical structure of DMA1 in Figure 1 was corrected on October 14, 2022. In the originally published version, DMA1 was missing a vinyl group on the left-hand side. This was due to a technical error when creating the high resolution image of Figure 1, and it has now been amended. This correction does not affect the overall results and conclusions of this.

Open access funding enabled and organized by Projekt DEAL.

Conflict of Interest

The authors declare no conflict of interest.

Data Availability Statement

The data that support the findings of this study are available from the corresponding author upon reasonable request.

Keywords

3D printing, block copolymers, fracture toughness, methacrylate resin, UV curing

Received: May 9, 2022
Revised: June 24, 2022
Published online: July 29, 2022

[1] P. Aly, C. Mohsen, *Eur. J. Dent.* **2020**, *14*, 189.
[2] A. Della Bona, V. Cantelli, V. T. Britto, K. F. Collares, J. W. Stansbury, *Dent. Mater.* **2021**, *37*, 336.
[3] M. S. Bilgin, A. Erdem, O. S. Aglarci, E. Dilber, *J. Prosthodontics* **2015**, *24*, 576.
[4] H. I. Yoon, H. J. Hwang, C. Ohkubo, J. S. Han, E. J. Park, *J. Prosthet. Dent.* **2018**, *120*, 919.
[5] H. J. Hwang, S. J. Lee, E. J. Park, H. I. Yoon, *J. Prosthet. Dent.* **2019**, *121*, 110.
[6] M. Forrest, W. D. Cook, A. A. Goodwin, F. Televantos, *Polym. Int.* **2001**, *50*, 53.
[7] H. Quan, T. Zhang, H. Xu, S. Luo, J. Nie, X. Zhu, *Bioact. Mater.* **2020**, *5*, 110.
[8] A. R. Kannurpatti, J. W. Anseth, C. N. Bowman, *Polymer* **1998**, *39*, 2507.
[9] N. Moszner, U. Salz, *Prog. Polym. Sci.* **2001**, *26*, 535.
[10] J. Slapnik, I. Pulko, *Prog. Addit. Manuf.* **2020**, *6*, 83.
[11] S. Beigi, H. Yeganeh, M. Atai, *Dent. Mater.* **2013**, *29*, 777.
[12] L. I. Chen, Q. Wu, G. Wei, R. Liu, Z. Li, *J. Mater. Chem. C* **2018**, *6*, 11561.
[13] R. A. Ranade, S. L. Wunder, G. R. Baran, *Polymer* **2006**, *47*, 4318.
[14] R. G. Hill, *J. Mater. Sci.* **1994**, *29*, 3062.
[15] V. A. Lee, H. L. Cardenas, H. R. Rawls, *J. Biomed. Mater. Res., Part B* **2010**, *94B*, 447.
[16] K. Pałka, J. Kleczewska, E. Sasimowski, A. Belcarz, A. Przekora, *Materials* **2020**, *13*, 2704.
[17] J. Jancar, K. Hynstova, V. Pavelka, *Compos. Sci. Technol.* **2009**, *69*, 457.
[18] D. Jagger, A. Harrison, R. Jagger, P. Milward, *J. Oral Rehabil.* **2003**, *30*, 231.
[19] P. Dorfinger, J. Stampfl, R. Liska, *Mater. Sci. Forum* **2015**, *825–826*, 53.
[20] B. Sandmann, B. Happ, I. Perevyazko, T. Rudolph, F. H. Schacher, S. Hoeppener, U. Mansfeld, M. D. Hager, U. K. Fischer, P. Burtscher, N. Moszner, U. S. Schubert, *Polym. Chem.* **2015**, *6*, 5273.
[21] M. Naguib, S. Grassini, M. Sangermano, *Macromol. Mater. Eng.* **2013**, *298*, 106.
[22] Y. Li, S. Peng, J. T. Miao, L. Zheng, J. Zhong, L. Wu, Z. Weng, *Chem. Eng. J.* **2020**, *394*, 124873.
[23] A. Gutiérrez-Mejía, W. Herrera-Kao, S. Duarte-Aranda, M. I. Loría-Bastarrachea, G. Canché-Escamilla, F. J. Moscoso-Sánchez, J. V. Cauich-Rodríguez, J. M. Cervantes-Uc, *Mater. Sci. Eng., C* **2013**, *33*, 1737.
[24] M. A. Hillmyer, P. M. Lipic, D. A. Hajduk, K. Almdal, F. S. Bates, *J. Am. Chem. Soc.* **1997**, *119*, 2749.
[25] T. Li, M. J. Heinzer, L. F. Francis, F. S. Bates, *J. Polym. Sci., Part B: Polym. Phys.* **2016**, *54*, 189.
[26] K. Utaloff, M. H. Kothmann, M. Ciesielski, M. Döring, T. Neumeyer, V. Altstädt, I. Gorman, M. Henningsen, *Polym. Eng. Sci.* **2019**, *59*, 86.
[27] E. Paz, J. Abenojar, Y. Ballesteros, F. Forriol, N. Dunne, J. C. Del Real, *J. Mater. Sci.: Mater. Med.* **2016**, *27*, 72.
[28] C. Uhlig, O. Kahle, O. Schäfer, D. Ewald, H. Oswaldbauer, J. Bauer, M. Bauer, *React. Funct. Polym.* **2019**, *142*, 159.
[29] J. Wu, Y. S. Thio, F. S. Bates, *J. Polym. Sci., Part B: Polym. Phys.* **2005**, *43*, 1950.
[30] D. H. Builes, A. Tercjak, *RSC Adv.* **2015**, *5*, 96170.
[31] J. Lequieu, A. J. D. Magenau, *Polym. Chem.* **2021**, *12*, 12.
[32] D. H. Builes, J. P. Hernández-Ortiz, M. A. Corcuera, I. Mondragon, A. Tercjak, *ACS Appl. Mater. Interfaces* **2014**, *6*, 1073.
[33] E. M. Redline, L. F. Francis, F. S. Bates, *J. Polym. Sci., Part B: Polym. Phys.* **2011**, *49*, 540.
[34] J. D. Liu, H. J. Sue, Z. J. Thompson, F. S. Bates, M. Dettloff, G. Jacob, N. Verghese, H. Pham, *Macromolecules* **2008**, *41*, 7616.
[35] M. Naguib, M. Sangermano, L. C. Capozzi, D. Pospiech, K. Sahre, D. Jehnichen, H. Scheibner, B. Voit, *Prog. Org. Coat.* **2015**, *85*, 178.
[36] E. R. Mafi, M. Ebrahimi, M. R. Moghbeli, *J. Polym. Eng.* **2009**, *29*, 293.
[37] H. J. Sue, P. M. Puckett, J. L. Bertram, L. L. Walker, *ACS Symp. Ser.* **2000**, *759*, 171.
[38] J. D. Liu, H. J. Sue, Z. J. Thompson, F. S. Bates, M. Dettloff, G. Jacob, N. Verghese, H. A. Pham, *Polymer* **2009**, *50*, 4683.
[39] F. Hübner, E. Szpoganicz, M. Demleitner, J. Kuhnigk, V. Altstädt, A. Rios De Anda, *ACS Appl. Polym. Mater.* **2020**, *2*, 4779.
[40] J. Yang, Q. Zhou, K. Shen, N. Song, L. Ni, *RSC Adv.* **2018**, *8*, 3705.
[41] W. Fan, L. Wang, S. Zheng, *Macromolecules* **2009**, *42*, 327.
[42] N. C. Das, G. T. Warren, C. C. Kao, B. G. Dragnea, P. Ni, P. E. Sokol, *Phys. Procedia* **2014**, *60*, 101.
[43] Y. Wei, M. J. A. Hore, *J. Appl. Phys.* **2021**, *129*, 171101.
[44] C. E. Corcione, R. Striani, M. Frigione, *Thermochim. Acta* **2014**, *576*, 47.
[45] T. Schlotthauer, J. Nitsche, P. Middendorf, *Rapid Prototyping J.* **2021**, *27*, 1910.

[46] C. Decker, *Acta Polym.* **1994**, *45*, 333.
[47] M. A. Gauthier, I. Stangel, T. H. Ellis, X. X. Zhu, *Biomaterials* **2005**, *26*, 6440.
[48] M. Miyazaki, H. Onose, N. Iida, H. Kazama, *Dent. Mater.* **2003**, *19*, 245.
[49] S. M. George, N. Hameed, S. Jose, J. J. George, J. Parameswaranpillai, in *Handbook of Epoxy Blends* (Eds: J. Parameswaranpillai, N. Hameed, J. Pionteck, E. Woo), Springer, Cham **2016**, pp. 1–34.
[50] M. Li, Z. Heng, Y. Chen, H. Zou, M. Liang, *Ind. Eng. Chem. Res.* **2018**, *57*, 13036.
[51] N. Hameed, Q. Guo, T. Hanley, Y. W. Mai, *J. Polym. Sci., Part B: Polym. Phys.* **2010**, *48*, 790.
[52] A. F. Senyurt, H. Wei, C. E. Hoyle, S. G. Piland, T. E. Gould, *Macromolecules* **2007**, *40*, 4901.
[53] H. Duan, W. Dong, X. Wang, X. Tao, H. Ma, *J. Appl. Polym. Sci.* **2019**, *136*, 48147.
[54] J. V. Crivello, E. Reichmanis, *Chem. Mater.* **2014**, *26*, 533.
[55] R. Anastasio, W. Peerbooms, R. Cardinaels, L. C. A. Van Breemen, *Macromolecules* **2019**, *52*, 9220.
[56] C. Ocando, A. Tercjak, E. Serrano, J. A. Ramos, S. Corona-Galván, M. D. Parellada, M. J. Fernández-Berridi, I. Mondragon, *Polym. Int.* **2008**, *57*, 1333.
[57] A. Klingler, A. Bajpai, B. Wetzel, *Eng. Fract. Mech.* **2018**, *203*, 81.
[58] L. Tao, Z. Sun, W. Min, H. Ou, L. Qi, M. Yu, *RSC Adv.* **2020**, *10*, 1603.
[59] M. T. Bashar, U. Sundararaj, P. Mertiny, *Polym. Eng. Sci.* **2014**, *54*, 1047.
[60] E. M. Redline, C. Declet-Perez, F. S. Bates, L. F. Francis, *Polymer* **2014**, *55*, 4172.
[61] R. Bagheri, B. T. Marouf, R. A. Pearson, *Polym. Rev.* **2009**, *49*, 201.
[62] Q. Guo, J. M. Dean, R. B. Grubbs, F. S. Bates, *J. Polym. Sci., Part B: Polym. Phys.* **2003**, *41*, 1994.
[63] Y. Kazuyoshi, H. Kishi, *J. Adhes. Soc. Jpn.* **2017**, *53*, 296.
[64] S. Bard, M. Demleitner, R. Weber, R. Zeiler, V. Altstädt, *Polymers* **2019**, *11*, 943.
[65] P. H. Mott, C. M. Roland, *Phys. Rev. B* **2009**, *80*, 132104.
[66] O. Glatter, O. Kratyk, *Small Angle X-ray Scattering*, Academic Press Inc. Ltd., San Diego, CA **1982**.

